Short baseline reactor $\bar{\nu} - e$ scattering experiments and nonstandard neutrino interactions at source and detector

Amir N. Khan*

Department of Physics, COMSATS IIT, Park Road, Islamabad 44000, Pakistan

Douglas W. McKay†

Department of Physics and Astronomy, University of Kansas, Lawrence, Kansas 66045, USA

F. Tahir‡

Department of Physics, COMSATS IIT, Park Road, Islamabad 44000, Pakistan

(Received 20 July 2014; published 16 September 2014)

We investigate nonstandard interaction effects in antineutrino-electron scattering experiments with baselines short enough to ignore standard oscillation phenomena. The setup is free of ambiguities from the interference between new physics and oscillation effects and is sensitive to both semileptonic new physics at the source and purely leptonic new physics in the weak interaction scattering at the detector. We draw on the TEXONO experiment as the model system, extending its analysis of nonstandard interaction effects at the detector to include the generally allowed nonstandard interaction phase at the detector and both nonuniversal and flavor-changing new physics at the reactor source. We confirm that the current data allows for new physics constraints at the detector of the same order as those currently published, but we find that constraints on the source new physics are at least an order of magnitude weaker. The new physics phase effects are at the 5% level, noticeable in the 90% C.L. contour plots but not significantly affecting the conclusions. Based on projected increase in sensitivity with an upgraded TEXONO experiment, we estimate the improvement of sensitivity to both source and detector nonstandard interactions. We find that the bounds on source parameters improve by an order of magnitude, but do not reach parameter space beyond current limits. On the other hand, the detector new physics sensitivity would push current limits by factors of 5 to 10 smaller.

DOI: 10.1103/PhysRevD.90.053008 PACS numbers: 13.15.+g, 14.60.St, 14.60.Pq

I. INTRODUCTION

In the past several years, reactor neutrino experiments [1–3] and long baseline accelerator experiments [4,5] have produced important advances in our understanding of neutrino mixing by measuring the key mixing parameter θ_{13} by two completely independent processes. The reactor experiments measure $\bar{\nu}_e$ disappearance in the flux of $\bar{\nu}_e s$, indicating oscillation into other neutrino flavors during the one or two kilometer trip from reactor core to detector. The accelerator experiment measures the appearance of a ν_e component in the ν_μ beam from an accelerator during the hundreds of kilometers trip from the accelerator laboratory to the detection site. Together, the results already constrain the CP-violating phase angle in the mixing matrix [4,5]. Moreover, the data provide a potentially powerful probe of nonstandard interactions (NSIs) [6] in the neutrino sector involving some combination of neutrino source, propagation, and detection [9–11].

In this paper, we explore the constraints on semileptonic, charged-current (CC), nonuniversal (NU) and flavor-changing (FC) NSI parameters and likewise for both NU and FC purely leptonic NSI parameters. The former appear in effective Lagrangians for neutrino production from reactors and from accelerators and for neutrino detection by inverse beta decay. The latter appear in neutrino production from muon decay and from neutrino detection by $\nu - e$ or $\bar{\nu} - e$ scattering. We will focus on the case of a *very* short baseline reactor $\bar{\nu}_e$ source and detection of the recoil electron from $\bar{\nu}_e + e \rightarrow \bar{\nu}_e + e$ scattering at the detector. We rely heavily on the example provided by the TEXONO experiment [12,13], which measures the recoil electron spectrum from reactor antineutrinos interacting with electrons in a CsI(Tl) detector. The baseline is less than 30 m, and the oscillation of the beam can be ignored, thus providing an especially clean test of FC "wrong flavor" $\bar{\nu}_\mu$ or $\bar{\nu}_\tau$ or NU "right flavor" $\bar{\nu}_e$ from the semileptonic nuclear decays in the reactor. Baselines this short avoid the degeneracies between NSI parameters and standard neutrino mixing parameters that occur in the analysis of data from reactor experiments with kilometer [1–3] or tens of kilometer baselines [14], degeneracies that are touched on in several recent studies [15–17].

*amir_nawaz@comsats.edu.pk
†dmckay@ku.edu
‡farida_tahir@comsats.edu.pk

We extend work in Ref. [13] by incorporating the effects of NSIs produced at the source and by including the phase dependence of the FC NSIs at the detector using the data from Texono's experiment. In Ref. [13], only the NSIs at the detector in the single channel of $\bar{\nu}_e - e$ scattering are considered. With NSIs at the source, there is a modification of the $\bar{\nu}_e$ component and an addition of $\bar{\nu}_\mu$ and $\bar{\nu}_\tau$ components, so $\bar{\nu}_\mu - e$ scattering and $\bar{\nu}_\tau - e$ scattering must be incorporated by including NSIs in the elastic, purely neutral current (NC), $\bar{\nu}_\mu - e$ and $\bar{\nu}_\tau - e$ cross sections, applicable for analyzing data from any short baseline neutrino scattering experiment where the oscillation effects are ignorable. Our "no NSI propagation effects" study complements those that probe NSIs with solar neutrino, accelerator neutrino, and other reactor neutrino experiments, which involve different combinations of NSIs at source, propagation, and detection effects [18–24].

In Secs. II, III, and IV, we define our notation, specify our cross sections, and define the flux factors that go with each cross section to unify all the standard model (SM) plus NSI contributions to the rate at source and detector in a single framework. Our formalism allows us to make joint confidence level (C.L.) contours with NSI parameters at source and at detector or at source alone and at detector alone. In Sec. IV, we apply this formalism to the TEXONO data and check key results from Refs. [12] and [13], while in Sec. V we apply the formalism to the modeled data based on the realistically achievable sensitivity proposed for an upgrade of the TEXONO experiment [25]. We recap and conclude in Sec. VI. Appendix A briefly summarizes the reactor flux and target density input to the recoil electron spectrum in the TEXONO experiment. Appendix B provides a table summarizing relevant model independent NSI parameter bounds from Ref. [11].

II. FORMALISM OF SOURCE AND DETECTOR NSIs

A. NSIs effective Lagrangians at source and detector

In the problem we address here, the source of antineutrinos is the semileptonic, CC decays of reactor nuclei. At the level of the quark content of the nucleons, the transition $d \to u + e + \bar{\nu}$ provides the antineutrinos for the elastic $\bar{\nu} - e$ scattering process at the detector. To allow for lepton-flavor-violating decays at the source, we adopt the semileptonic, CC, effective Lagrangian [15,26,27]

$$\mathcal{L}^s = -2\sqrt{2}G_F(\delta_{\alpha\beta} + K_{\alpha\beta})(\bar{l}_\alpha \gamma_\lambda P_L U_{\beta a}\nu_a)(\bar{d}\gamma^\lambda P_L u)^\dagger + \text{H.c.}, \tag{1}$$

where repeated flavor-basis indices "α" and "β" and mass-basis indices "a" are summed over. We confine ourselves to the left-handed quark helicity projection case for simplicity. The inclusion of the right-handed terms adds nothing essential to our discussion. Since we consider neutrino-propagation baselines that are only a few tens of meters and energies that are in the few MeV range, oscillations play no role and we can effectively replace $U_{\beta a}\bar{\nu}_a \to \bar{\nu}_\beta$ in making the rate calculations we present here. The complex coefficients $K_{\alpha\beta}$ represent the relative coupling strengths of the flavor combinations in the presence of new physics, while in the SM, $K_{\alpha\beta} = 0$.

To represent the NSI effects in the purely leptonic sector [26–30] for the simplified elastic $\bar{\nu} - e$ scattering case of interest, we write the effective Lagrangian as

$$\begin{aligned}\mathcal{L}^\ell &= \mathcal{L}^\ell_{\text{NU}} + \mathcal{L}^\ell_{\text{FC}} \\ &= -2\sqrt{2}G_F \sum_\alpha (\bar{e}\gamma_\mu(\tilde{g}_{\alpha R}P_R + (\tilde{g}_{\alpha L}+1)P_L)e)(\bar{\nu}_\alpha\gamma^\mu P_L \nu_\alpha) \\ &\quad -2\sqrt{2}G_F \sum_{\alpha\neq\beta} \varepsilon^{eP}_{\alpha\beta}(\bar{e}\gamma_\lambda P e)(\bar{\nu}_\alpha \gamma^\lambda P_L \nu_\beta).\end{aligned} \tag{2}$$

The first term in Eq. (2) is the NU case and the second term is the FC case. The coefficients $\tilde{g}_{\alpha R}$ and $\tilde{g}_{\alpha L}$ are

$$\tilde{g}_{\alpha R} = \sin^2\theta_w + \varepsilon^{eR}_{\alpha\alpha} \quad \text{and} \quad \tilde{g}_{\alpha L} = \sin^2\theta_w - \frac{1}{2} + \varepsilon^{eL}_{\alpha\alpha}. \tag{3}$$

Hermiticity of $\mathcal{L}^\ell$ requires that the NSI matrix of parameters be Hermitian: $\epsilon^{eR,L}_{\alpha\beta} = (\epsilon^{eR,L}_{\beta\alpha})^*$, so the FC NSI parameters are complex in general. Adopting the commonly used "ε" notation for the leptonic sector makes the distinction between source (Ks) and detector (εs) clear. With the effective Lagrangians defined, we are now ready to summarize the cross sections and flux factors we need for the study of the NSI effects at source and detector.

B. $\bar{\nu}_e - e$, $\bar{\nu}_\mu - e$ and $\bar{\nu}_\tau - e$ differential scattering cross sections in lab frame

In the notation for the NSI terms defined in Eq. (2) above, the differential cross section for the $\bar{\nu}_e - e$ scattering with neutrino lab energy E$_\nu$ and recoil electron kinetic energy T can be summarized by the expression

$$\begin{aligned}\left[\frac{d\sigma(\bar{\nu}_e e)}{dT}\right]_{\text{SM+NSI}} &= \frac{2G_F^2 m_e}{\pi}\Bigg[\tilde{g}^2_{eR} + \sum_{\alpha\neq e}|\varepsilon^{eR}_{\alpha e}|^2 \\ &\quad + ((\tilde{g}_{eL}+1)^2 + \sum_{\alpha\neq e}|\varepsilon^{eL}_{\alpha e}|^2)\left(1-\frac{T}{E_\nu}\right)^2 \\ &\quad - (\tilde{g}_{eR}(\tilde{g}_{eL}+1) + \sum_{\alpha\neq e}\Re[(\varepsilon^{eR}_{\alpha e})^*\varepsilon^{eL}_{\alpha e}])\frac{m_e T}{E_\nu^2}\Bigg],\end{aligned} \tag{4}$$

which is the sum of the scattering cross sections for the three, incoherent processes $\bar{\nu}_e + e \to \bar{\nu}_e \to e$, $\bar{\nu}_e + e \to \bar{\nu}_\mu + e$, and $\bar{\nu}_e + e \to \bar{\nu}_\tau + e$. The $\bar{\nu}_e + e \to \bar{\nu}_e + e$ cross section is represented by the terms containing the $\tilde{g}_{eL}$ and $\tilde{g}_{eR}$ parameters. It is the coherent sum of the NC and CC contributions. The complex parameters $\varepsilon^{eL}_{\alpha e}$, where $\alpha \neq e$, can be written either as $\varepsilon_{\alpha e}^{eL} = \Re[\varepsilon_{\alpha e}^{eL}] + i\Im[\varepsilon_{\alpha e}^{eL}]$ or as $|\varepsilon_{\alpha e}^{eL}|\exp(i\phi_{\alpha e}^{eL})$, where $\phi_{\alpha e}^{eL}$ is the phase angle of the complex quantity. Written out in more detail, the NSI contributions are $|\varepsilon_{\alpha e}^{eR}|^2 = (\Re[\varepsilon_{\alpha e}^{eR}])^2 + (\Im[\varepsilon_{\alpha e}^{eR}])^2$, and similarly for $R \to L$. In the last term, $\Re[(\varepsilon_{\alpha e}^{eR})^* \varepsilon_{\alpha e}^{eL}] = \Re[\varepsilon_{\alpha e}^{eR}]\Re[\varepsilon_{\alpha e}^{eL}] + \Im[\varepsilon_{\alpha e}^{eR}]\Im[\varepsilon_{\alpha e}^{eL}]$. This notation makes it clear that when the ε parameters are taken as real positive or negative, then the "$\Re$" and "$\Im$" notations can be dropped and one can drop the absolute magnitude signs everywhere. All of the NSI studies with $\nu - e$ or $\bar{\nu} - e$ scattering at the detector tacitly make this assumption [13,18–21,24]. If the parameters are written as $|\varepsilon_{\alpha e}^{eL}|\exp(i\phi_{\alpha e}^{eL})$ and $|\varepsilon_{\alpha e}^{eR}|\exp(i\phi_{\alpha e}^{eR})$, then the coefficient in the last term can be expressed as

$$\Re[(\varepsilon_{\alpha e}^{eR})^* \varepsilon_{\alpha e}^{eL}] = |\varepsilon_{\alpha e}^{eR}||\varepsilon_{\alpha e}^{eL}|\cos(\phi_{\alpha e}^{eL} - \phi_{\alpha e}^{eR}). \tag{5}$$

With this parametrization, the values of $|\varepsilon_{\alpha e}^{eR}|$ and $|\varepsilon_{\alpha e}^{eL}|$ are always positive and the sign of the term is controlled by $\cos(\phi_{\alpha e}^{eL} - \phi_{\alpha e}^{eR})$.

To include the NSIs at the reactor source, using the notation from [15], one multiplies the contribution to the rate by $|1 + K_{ee}|^2$. Though Ref. [15] works only to first order in NSI parameters and drops the highly constrained linear term $2\Re[K_{ee}]$ [11], in the present calculation we must work to second order to assess the impact of the NSIs, so *both* $\Im[K_{ee}]$ and $\Re[K_{ee}]$ will be included in the NU case $\bar{\nu}_e + e \to \bar{\nu}_e + e$.

For the other incoming neutrino flavors, we multiply the $\bar{\nu}_\mu - e$ cross section by the factor $|K_{e\mu}|^2$for the $\bar{\nu}_\mu$ component of the flux and by $|K_{e\tau}|^2$ for the $\bar{\nu}_\tau$ component. The $\bar{\nu}_\mu - e$ differential cross section is

$$\left[\frac{d\sigma(\bar{\nu}_\mu e)}{dT}\right]_{\text{SM+NSI}} = \frac{2G_F^2 m_e}{\pi}\left[\tilde{g}_{\mu R}^2 + \sum_{\alpha\neq\mu}|\varepsilon_{\alpha\mu}^{eR}|^2 + \left(\tilde{g}_{\mu L}^2 + \sum_{\alpha\neq\mu}|\varepsilon_{\alpha\mu}^{eL}|^2\right)\left(1 - \frac{T}{E_\nu}\right)^2 - \left(\tilde{g}_{\mu R}\tilde{g}_{\mu L} + \sum_{\alpha\neq\mu}\Re[(\varepsilon_{\alpha\mu}^{eR})^*\varepsilon_{\alpha\mu}^{eL}]\right)\frac{m_e T}{E_\nu^2}\right]. \tag{6}$$

The cross section for $\bar{\nu}_\tau - e$ scattering is obtained by replacing μ by τ everywhere in the above equation. The definitions of $\tilde{g}_{\mu R,\mu L}$ and $\tilde{g}_{\tau R,\tau L}$ are obvious counterparts to the definition of $\tilde{g}_{eR,eL}$ in Eq. (3).

C. Discussion of NSIs at the source and the full NSI effects

The distance between the source and detector in the TEXONO experiment is less than 30 m, so we will use the fact that the oscillation effects, proportional to $\sin^2(m_i^2 - m_j^2)L/4E_\nu$, are ignorable for the range of interest, 3 MeV $\leq E_\nu \leq$ 8 MeV. In effect, this means that the flavor of neutrino that is produced at the source is the same as the flavor that reaches the detector. The factors that control the flux of each flavor in the incoming beam produced at the source are the $K_{\alpha\beta}$. The TEXONO flux model is the result of a large number of independent nuclear reactions. In the presence of NSIs, the emitted flux can be thought of as an incoherent sum of $\bar{\nu}_e$, $\bar{\nu}_\mu$, and $\bar{\nu}_\tau$ with weights $|1 + K_{ee}|^2$, $|K_{e\mu}|^2$, and $|K_{e\tau}|^2$. The source and detector NSI effects on the rate are then expressed through the following factor, denoted by $\mathcal{F}$, that will multiply the reactor flux and the target electron number density to get the differential rate $\frac{dR_X}{dT}$, as described in Appendix A:

$$\mathcal{F} = |1 + K_{ee}|^2\left[\frac{d\sigma(\overline{\nu_e}e)}{dT}\right] + |K_{e\mu}|^2\left[\frac{d\sigma(\bar{\nu}_\mu e)}{dT}\right] + |K_{e\tau}|^2\left[\frac{d\sigma(\bar{\nu}_\tau e)}{dT}\right], \tag{7}$$

where the cross section formulas are as given in Eqs. (4) and (6) and the SM plus NSI designation is understood.

III. PROBING MODEL PARAMETERS WITH RECOIL ELECTRON ENERGY SPECTRUM DATA: THE TEXONO EXPERIMENT

We reproduce and recap the TEXONO experiment [12] and its related analyses [13,25] that are directly relevant to our NSI parameters study. The neutrino flux spectrum and the event rate data and its theoretical representation are briefly summarized in Appendix A. In Ref. [12], the primary goal was an independent determination of the weak mixing parameter $\sin^2\theta_W$, determined strictly from low energy, purely leptonic recoil spectrum data in the $\bar{\nu}_e + e \to \bar{\nu}_e + e$ elastic scattering process. The paper stresses that this data is more sensitive to the right-handed NC component in Eq. (4) than is the corresponding $\nu_e + e \to \nu_e + e$ scattering case, where the roles of g_L and g_R are reversed. The $\bar{\nu}_e - e$ scattering is consequently more sensitive to $g_R = \sin^2\theta_W$. Using their flux and binned rate spectrum [31], we show the result of a χ^2 analysis with statistical errors only in Fig. 1(a). The 1σ and 90% C.L. lines are included for guidance. We find a best fit of $\sin^2\theta_W = 0.251 \pm 0.030$ in agreement with TEXONO's result.

Following publication of their experimental results [12] detailing the experiment and the results on $\sin^2\theta_W$ and on an upper limit of the neutrino magnetic moment, the collaboration presented limits on NSI parameters and on couplings of unparticles to neutrinos and electrons [13]. Since we are pursuing an extension of the NSI bounds to include the possibility of semileptonic NSI modifications to the reactor source of $\bar{\nu}_e$s and the interplay with the purely leptonic detection NSIs, we are primarily interested in C.L. boundaries in two-parameter fits to the data and the joint limits obtained from these analyses. For illustration, we

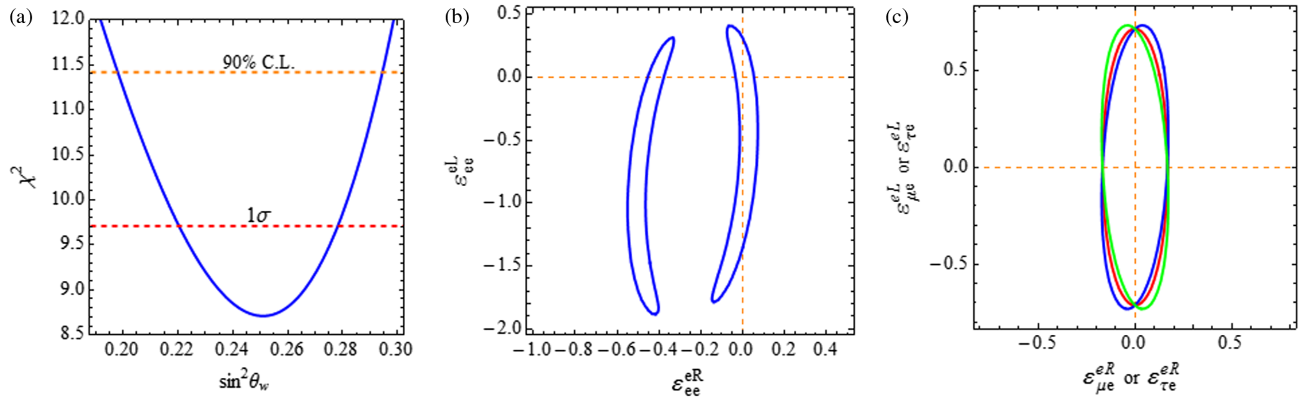

FIG. 1 (color online). SM $\sin^2\theta_W$ vs χ^2, 1(a), and our calculation of the 90% C.L. limits of Figs. 4(a) and 4(b) of Ref. [15] in Figs. 1(b) and 1(c). In Fig. 1(c), we show the 90% C.L. boundary for the fit to TEXONO rate data using Eq. (5) in the scattering cross section Eq. (2). The blue, red, and green curves, right to -left at the top, are for $\cos(\phi_{\alpha e}^{eL} - \phi_{\alpha e}^{eR}) = 1, 0$, and -1, respectively. The blue curve, with $\cos(\phi_{\alpha e}^{eL} - \phi_{\alpha e}^{eR}) = 1$, corresponds to that shown in Fig. 4(c) of Ref. [15].

check our evaluation of the 90% C.L. boundaries in the $\epsilon_{ee}^{eR} - \epsilon_{ee}^{eL}$ plane and, alternatively, the $\epsilon_{e\tau}^{eR} - \epsilon_{e\tau}^{eL}$ plane, Figs. 4(a) and 4(b) in [13]. We show the result of this exercise in Figs. 1(b) and the blue boundary, rightmost at the top, in Fig. 1(c). In both cases we find that our results and TEXONO's agree within the ability to read off values along the contours. We show the 90% C.L. projections of these plots on the individual axes for the two cases in Table I. The red and green curves, center and leftmost in Fig. 1(c), are examples of other phase choices, as we discuss in Sec. III A. For the NU case of the $\epsilon_{ee}^{eR} - \epsilon_{ee}^{eL}$ plane, we quote the right-hand solution values, since both the R and L limits are the most stringent for this solution. The FC case assumes the NSI parameters are purely real. There is no degeneracy in this case, and the projected individual two-parameter limits are straightforward. The weak correlation between the R- and L- NSI parameters is due to the small R-L NSI interference term. Though our contour agrees with that as obtained in Ref. [13] and our $\epsilon_{\tau e}^{eR}$ bounds agree with the ones quoted in their Table I, our limits on $\epsilon_{\tau e}^{eL}$ are somewhat smaller.

A. Role of the detector NSI phases in determining the C.L. boundaries

The R-L interference term in the differential cross sections depends on the FC NSI parameter phases, as displayed for the case $\bar{\nu}_e + e \to \bar{\nu} + e$ in Eq. (5). From the point of view of this general formula, the blue boundary, rightmost at the top, in Fig. 1(c) can be interpreted as the composite of the cases $\phi_{\mu e}^{eR} = \phi_{\mu e}^{eL} = 0$, where $\epsilon_{\mu e}^{eR}$ and $\epsilon_{\mu e}^{eL}$ are both real and positive, $\phi_{\mu e}^{eR} = \pi$ and $\phi_{\mu e}^{eL} = 0$, where $\epsilon_{\mu e}^{eR}$ is real and negative and $\epsilon_{\mu e}^{eL}$ is real and positive, $\phi_{\mu e}^{eR} = \phi_{\mu e}^{eL} = \pi$, where $\epsilon_{\mu e}^{eR}$ and $\epsilon_{\mu e}^{eL}$ are both real and negative, and, finally, $\phi_{\mu e}^{eR} = 0$ and $\phi_{\mu e}^{eL} = \pi$, where $\epsilon_{\mu e}^{eR}$ is real and positive and $\epsilon_{\mu e}^{eL}$ is real and negative. Alternatively, it can be interpreted as the composite of cases where 0 and π are replaced with $\pi/2$ and $3\pi/2$ and real replaced with imaginary. Because the R-L interference term is suppressed by the factor $m_e T/E_\nu^2$ and $E_\nu \geq 3$ MeV, the changes in the parameter boundaries as the phase differences range from 0 to π are small, as shown in Fig. 1(c). Conclusions about allowed boundaries for NSI parameters for the range of energies of interest in reactor experiments are affected very little in this analysis, but for experiments with significantly lower energy radioactive sources or for low energy solar neutrino experiments such as Borexino [32], the R-L correlation term can be relatively larger and the phase effects may be important. For present purposes, we illustrate the range of effects that change of phases can make on the C.L. boundary in Fig. 1(c). The small changes in boundaries are shown in the figure by the difference between the blue, red, and green curves, corresponding to $\cos(\phi_{\alpha e}^{eL} - \phi_{\alpha e}^{eR}) = 1$, 0, and -1, reading from right to left at the top of the figure. As one sees, the correlation disappears for the case that $\cos(\phi_{\alpha e}^{eL} - \phi_{\alpha e}^{eR}) = 0$, the red, middle curve. The R-L correlation term vanishes in this case because the R- and L-parameters are $\pi/2$ out of phase; one can be real and the other imaginary, for example.

TABLE I. Bounds at 90% C.L. obtained from Figs. 1(b) and 1(c) in the absence of any source NSIs where $\alpha = \mu$ or τ.

Figure no.	R-parameter bounds	L-parameter bounds
1(b)	$-0.15 < \epsilon_{ee}^{eR} < 0.08$	$-1.79 < \epsilon_{ee}^{eL} < 0.41$
1(c)	$-0.18 < \epsilon_{\alpha e}^{eR} < 0.18$	$-0.76 < \epsilon_{\alpha e}^{eL} < 0.76$

IV. INTERPLAY BETWEEN $K_{\alpha\beta}$ (SOURCE) AND $\epsilon_{\alpha\beta}^{eR,L}$ (DETECTOR) NSI PARAMETERS

In this section we take pairs of source and detector NSI coefficients to survey the 90% C.L. boundaries in the various two-parameter spaces. We focus on the bounds

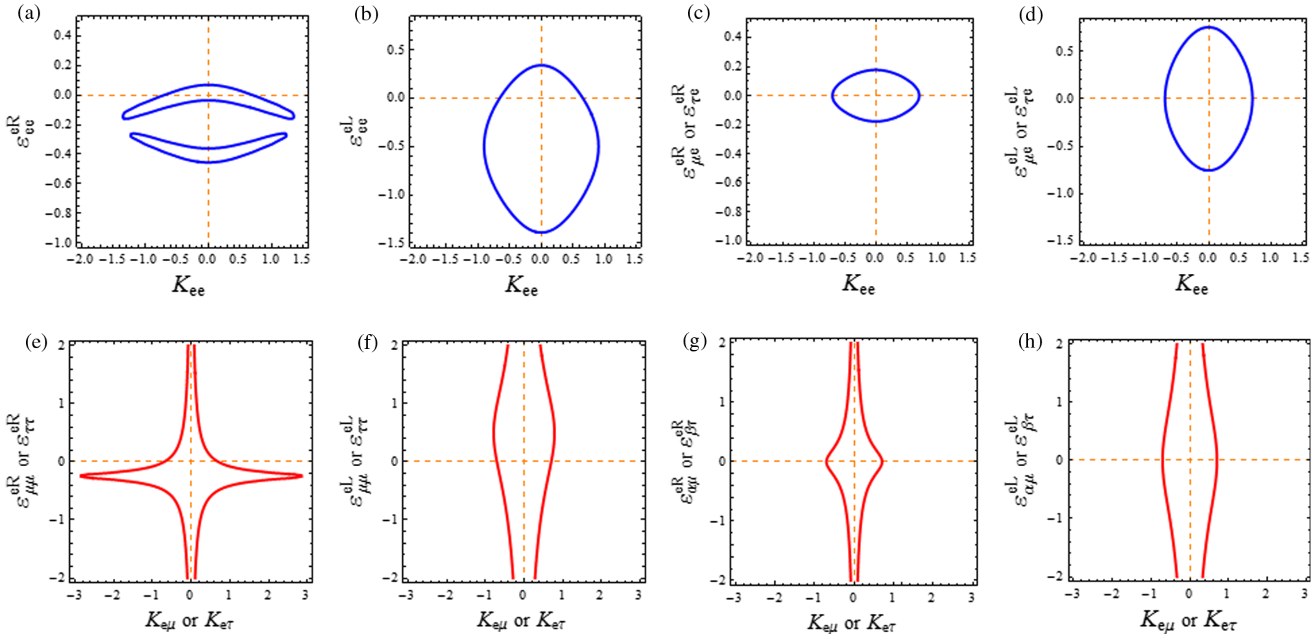

FIG. 2 (color online). C.L. boundary regions for published TEXONO data. Upper panels [(a)–(d)]: Correlation between the source NSI parameters (K_{ee}) and the corresponding detector NSI parameters ($\varepsilon^{R,L}_{ee}$ and $\varepsilon^{R,L}_{\alpha e}$, where $\alpha = \mu$ or τ) at 90% C.L. See the text for details. Lower panels [(e)–(h)]: Correlation between the source NSI parameters ($K_{e\alpha}$) and the corresponding detector NSI parameters ($\varepsilon^{R,L}_{\mu\mu}$, $\varepsilon^{R,L}_{\tau\tau}$ and $\varepsilon^{R,L}_{\alpha\mu}$, $\varepsilon^{R,L}_{\beta\tau}$, where $\alpha = e$ or τ and $\beta = e$ or μ) at 90% C.L. See the text for details.

on the source parameters and assess the strength of the bounds found to the bounds currently available in the literature. At the same time, we check for consistency of the bounds on the detector NSI parameters with those found by TEXONO [13], which we checked in the preceding section.

Since the current bounds on the real part of K_{ee} are of the order 10^{-3}, as given in Ref. [11] and found independently from Daya Bay data in Ref. [17], and these are much tighter than we can imagine providing with the current analysis based on the TEXONO data, we assume K_{ee} is purely imaginary in this section. Consequently, the source coefficient in the case of incident $\bar{\nu}_e$ in Eq. (7) is $K^2_{ee} = 1 + (\Im[K_{ee}])^2$. Bounds found will then refer to $\Im[K_{ee}]$. Figure 2 shows the 90% C.L. boundaries for the fits to the TEXONO data as parametrized by one source NSI coefficient and one detector coefficient with all of the other NSI coefficients set to zero. From the 90% C.L. contours shown in Fig. 2, we can determine the 90% C.L. bounds on the source NU K_{ee} parameter and any of the $\epsilon^{eR,L}_{\alpha e}$ at the detector by projecting onto the parameter axes for each contour. We find the limits on the NU parameters quoted in Table II. In all of the cases involving the source FC semileptonic NSI parameters $K_{\alpha\beta}$, there is no bound on any of the leptonic, detector NSI parameters $\epsilon^{eR,L}_{\alpha\beta}$ as $K_{\alpha\beta} \to 0$, because the source is receiving only $\bar{\nu}_e$ flux in this limit. In this sense, the parameters $K_{\alpha\beta}$ and $\epsilon^{eR,L}_{\alpha\beta}$ are highly correlated. There is still the possibility for placing upper bounds on the $K_{e\alpha}$ parameters in this case if the

TABLE II. Bounds at 90% C.L. obtained from Fig. 2 where $\alpha = e$ or τ and $\beta = e$ or μ.

Figure no.	NSI parameters at source	NSI parameters at detector
2(a)	$-1.35 < \mathrm{Im}K_{ee} < 1.35$	$-0.17 < \varepsilon^{eR}_{ee} < 0.07$
2(b)	$-0.9 < \mathrm{Im}K_{ee} < 0.9$	$-1.4 < \varepsilon^{eL}_{ee} < 0.34$
2(c)	$-0.72 < \mathrm{Im}K_{ee} < 0.72$	$-0.18 < \varepsilon^{eR}_{\alpha e} < 0.18$
2(d)	$-0.72 < \mathrm{Im}K_{ee} < 0.72$	$-0.76 < \varepsilon^{eL}_{\alpha e} < 0.76$
2(e)	$-0.72 < \mathrm{Im}K_{e\mu}$ or $\mathrm{Im}K_{e\tau} < 0.72$	$\varepsilon^{eR}_{\mu\mu}$ and $\varepsilon^{eR}_{\tau\tau}$ are unbounded
2(f)	$-0.72 < \mathrm{Im}K_{e\mu}$ or $\mathrm{Im}K_{e\tau} < 0.72$	$\varepsilon^{eL}_{\mu\mu}$ and $\varepsilon^{eL}_{\tau\tau}$ are unbounded
2(g)	$-0.72 < \mathrm{Im}K_{e\mu}$ or $\mathrm{Im}K_{e\tau} < 0.72$	$\varepsilon^{eR}_{\alpha\mu}$ and $\varepsilon^{eR}_{\beta\tau}$ are unbounded
2(h)	$-0.72 < \mathrm{Im}K_{e\mu}$ or $\mathrm{Im}K_{e\tau} < 0.72$	$\varepsilon^{eL}_{\alpha\mu}$ and $\varepsilon^{eL}_{\beta\tau}$ are unbounded

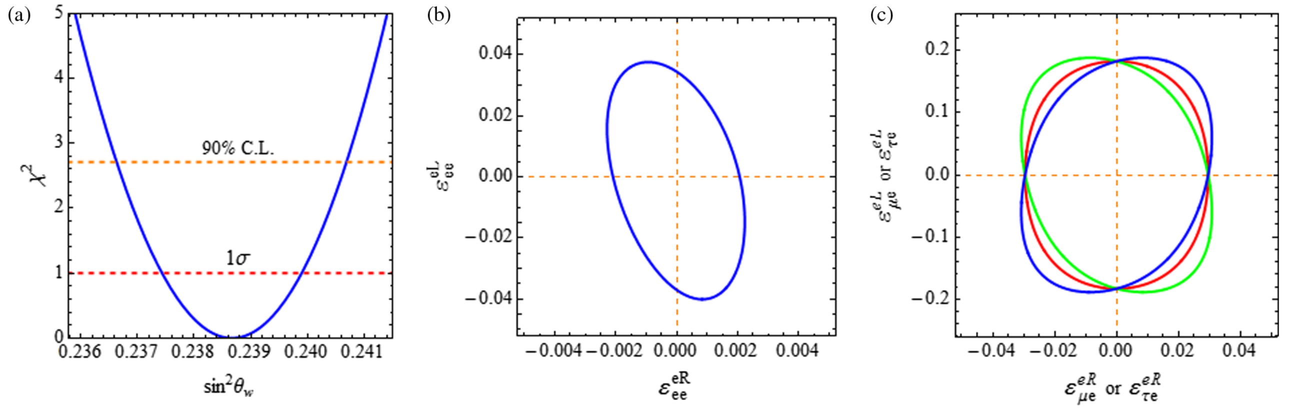

FIG. 3 (color online). SM $\sin^2\theta_W$ vs χ^2, (a), the 90% C.L. contour for NU L- and R-NSI parameters, (b), and in (c) the 90% C.L. contours for the same phase choices as in Fig. 1, but for the modeled future prospects data. All source NSI parameters are set to zero.

detector NSI parameters are constrained to be smaller than their current bounds [11], which are near zero on the scale of Fig. 2. We can then place upper 90% C.L. bounds on the values of $K_{e\mu}$ or $K_{e\tau}$ for the special case where detector NSIs $\epsilon^{eR,L}_{\mu\mu} = \epsilon^{eR,L}_{\alpha\mu} = 0$, and likewise for $\mu \to \tau$. These one-parameter-at-a time upper bounds on $K_{e\mu}$ or $K_{e\tau}$, the type commonly reported in the literature, are the bounds we quote in Table II [33]. Because only $\epsilon^{eR}_{\mu e}$ is taken to be nonzero in the two-parameter analysis yielding Fig. 2(c), there is no dependence on its phase, and similarly for $\epsilon^{eL}_{\mu e}$ in Fig. 2(d). As indicated in Eq. (5) and illustrated in Fig. 1(c), both must be included in a fitting analysis for the relative phase to play a role.

Briefly summarized, the results of this study based on the published TEXONO data show that the sensitivity to reactor *source* NSIs, $K_{\alpha\beta}$, is at least an order of magnitude less than the sensitivity of the data used to establish the currently available bounds. On the other hand, the sensitivity to *detector* NSIs is of the same order of magnitude as the current bounds for the right-handed NSI couplings, though much less for the left-handed couplings. The future improvements in sensitivity, as envisioned by the TEXONO Collaboration [13,25], should change this situation considerably, and we turn to this consideration in the next section.

V. FUTURE PROSPECTS

In this section we study the future prospects for tightening the source and detector NSI parameter bounds by adopting the projected "realistic and feasible" improvements in statistical sensitivities reported in Table 2 and the related text in Ref. [25]. Their essential point is that statistical uncertainty of the measured value of $\sin^2\theta_W$ can realistically be reduced to ± 0.0013. We follow the experimental setup from Refs. [12,13] and generate our data in 10 energy bins, each of step 0.5 Mev . We generate our "data model" by assuming that the best fit value turns out to be $\sin^2\theta_W = 0.2387$ [34], the value cited for comparison to their experimental fit value $\sin^2\theta_W = 0.251$ by Ref. [12]. We define our model χ^2-distribution by forming

$$\chi^2 = \sum_i \left(\frac{R_{\rm NSI} - R_{\rm SM}}{\Delta_{\rm stat}}\right)^2_i \tag{8}$$

where $R_{\rm SM}$ is the data model rate, $R_{\rm NSI}$ is the predicted event rate with all unknown NSI parameters and $\Delta_{\rm stat}$ is the statistical uncertainty over each bin. We define $\Delta_{\rm stat}$ as the deviation from the central value $R_{\rm SM}$ within 1σ statistical uncertainty, obtained by evaluating the rate with $\sin^2\theta_W = 0.2387$. To achieve a fit to the 10 bins of rate data that yields the projected uncertainty of ± 0.0013 for $\sin^2\theta_W$, we find that evaluating the rates in each bin with $\sin^2\theta_W$ roughly $(\sqrt{10} \simeq 3) \times \pm 0.0013$ per bin and taking the average deviation from the central value yields a data set whose uncertainties are consistent with expectations [25]. We take this model set as the basis for estimated future sensitivity to NSIs [24]. The results shown in Fig. 1 are redone using future prospects data in Fig. 3 and the bounds obtained at 90% C.L. are given in Table III [24].

From Fig. 3 and the bounds summarized in Table III, we see immediately the impact of improved sensitivity to the presence of NSIs at the detector in the removal of the degeneracy in the ϵ^{eR}_{ee} vs ϵ^{eL}_{ee} plot when compared to Fig. 1. The purely leptonic NU and FC new physics effects can be probed with up to 2 orders of magnitude higher refinement in the right-handed lepton sector and up to an order of magnitude more refinement in the left-handed sector. With comparable experimental sensitivity in a $\nu_e + e \to \nu_e + e$

TABLE III. Bounds at 90% C.L. obtained from Figs. 3(b) and 3(c) in the absence of any source NSIs where $\alpha = \mu$ or τ.

Figure no.	R-parameter bounds	L-parameter bounds
3(b)	$-0.0023 < \epsilon^{eR}_{ee} < 0.0023$	$-0.04 < \epsilon^{eL}_{ee} < 0.04$
3(c)	$-0.03 < \epsilon^{eR}_{\alpha e} < 0.03$	$-0.19 < \epsilon^{eL}_{\alpha e} < 0.19$

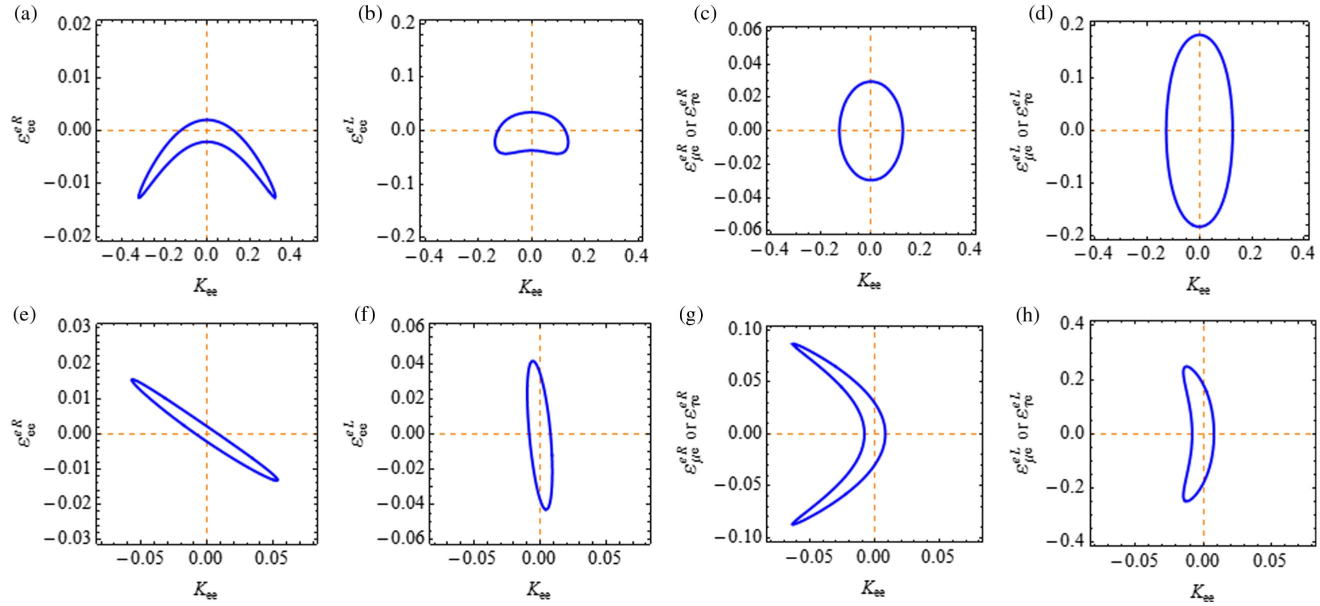

FIG. 4 (color online). C.L. boundary regions for *future prospects* data. Upper panels [(a)–(d)]: Correlation between the source NSI parameter (ImK_{ee}) and the corresponding detector NSI parameters ($\varepsilon_{ee}^{R,L}$ and $\varepsilon_{\alpha e}^{R,L}$, where $\alpha = \mu$ or τ) at 90% C.L. See the text for details. Lower panels [(e)–(h)]: Correlation between the source NSI parameter (ReK_{ee}) and the corresponding detector NSI parameters ($\varepsilon_{\mu\mu}^{R,L}$, $\varepsilon_{\tau\tau}^{R,L}$ and $\varepsilon_{\alpha\mu}^{R,L}$, $\varepsilon_{\beta\tau}^{R,L}$ where $\alpha = e$ or τ and $\beta = e$ or μ) at 90% C.L. See the text for details.

experiment, a complementary result with the *left-handed* sector being favored could be achieved [35,36] .

Turning to the cases where the NSIs can be active at *both* the source and detector, we study the parameter spaces of combined source-detector pairs in Fig. 4 and in accompanying Table IV. The sensitivity to the combinations improves typically by factors of 5 to 10 in both source and detector probes compared to the bounds shown in Fig. 2 and Table II. Comparing to current bounds in our Appendix B, Table VII, for example, we find that the bound on ε_{ee}^{eR} in entry 4(e) is a factor of 10 below the bound given there, while the bound on $\varepsilon_{\tau e}^{eR}$ given in entry 4(g) is a factor of 5 below its bound quoted in [11]. In the case of NU K_{ee} couplings, the constraints

TABLE IV. Bounds at 90% C.L. obtained from Fig. (4) where $\alpha = e$ or τ and $\beta = e$ or μ.

Figure no.	NSI parameters at source	NSI parameters at detector
4(a)	$-0.33 < \mathrm{Im}K_{ee} < 0.33$	$-0.013 < \varepsilon_{ee}^{eR} < 0.002$
4(b)	$-0.14 < \mathrm{Im}K_{ee} < 0.14$	$-0.045 < \varepsilon_{ee}^{eL} < 0.036$
4(c)	$-0.13 < \mathrm{Im}K_{ee} < 0.13$	$-0.03 < \varepsilon_{\alpha e}^{eR} < 0.03$
4(d)	$-0.13 < \mathrm{Im}K_{ee} < 0.13$	$-0.18 < \varepsilon_{\alpha e}^{eL} < 0.18$
4(e)	$-0.057 < \mathrm{Re}K_{ee} < 0.054$	$-0.013 < \varepsilon_{ee}^{eR} < 0.016$
4(f)	$-0.01 < \mathrm{Re}K_{ee} < 0.01$	$-0.043 < \varepsilon_{ee}^{eL} < 0.042$
4(g)	$-0.064 < \mathrm{Re}K_{ee} < 0.007$	$-0.086 < \varepsilon_{\alpha e}^{eR} < 0.086$
4(h)	$-0.015 < \mathrm{Re}K_{ee} < 0.008$	$-0.25 < \varepsilon_{\alpha e}^{eL} < 0.25$

TABLE V. Bounds obtained from Fig. (5) at 90% C.L. where $\alpha = e$ or τ and $\beta = e$ or μ. All the source NSI parameters $K_{\alpha\beta}$ are either pure real or imaginary.

Figure no.	NSI parameters at source	NSI parameters at detector
5(a)	$-0.1 < K_{e\mu}$ or $K_{e\tau} < 0.1$	$\varepsilon_{\mu\mu}^{eR}$ and $\varepsilon_{\tau\tau}^{eR}$ are unbounded
5(b)	$-0.1 < K_{e\mu}$ or $K_{e\tau} < 0.1$	$\varepsilon_{\mu\mu}^{eL}$ and $\varepsilon_{\tau\tau}^{eL}$ are unbounded
5(c)	$-0.1 < K_{e\mu}$ or $K_{e\tau} < 0.1$	$\varepsilon_{\alpha\mu}^{eR}$ and $\varepsilon_{\beta\tau}^{eR}$ are unbounded
5(d)	$-0.1 < K_{e\mu}$ or $K_{e\tau} < 0.1$	$\varepsilon_{\alpha\mu}^{eL}$ and $\varepsilon_{\beta\tau}^{eL}$ are unbounded

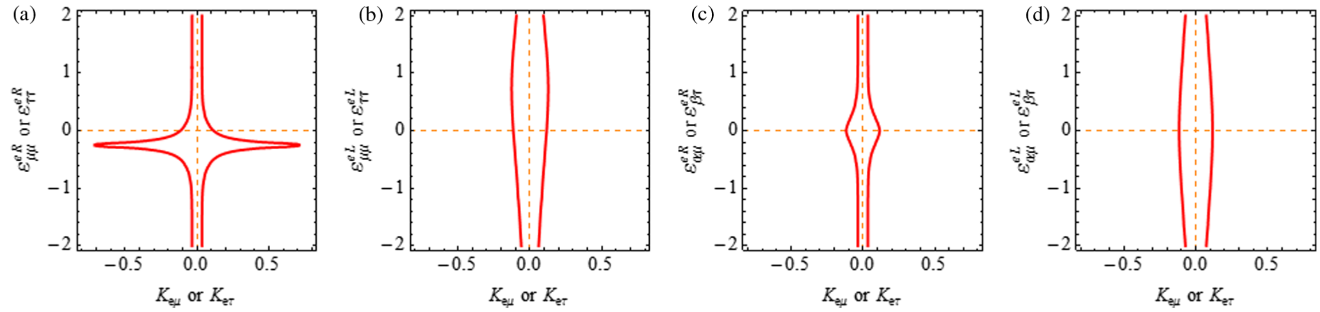

FIG. 5 (color online). Correlation between the source NSI parameters ($\mathrm{Re}K_{e\mu}$ and $\mathrm{Re}K_{e\tau}$) and the corresponding detector NSI parameters ($\varepsilon^{R,L}_{\mu\mu}$, $\varepsilon^{R,L}_{\tau\tau}$ and $\varepsilon^{R,L}_{\alpha\mu}$, $\varepsilon^{R,L}_{\beta\tau}$ where $\alpha = e$ or τ and $\beta = e$ or μ) at 90% C.L. See the text for details.

are becoming competitive with those published [11], being within about a factor of 3 for both the imaginary part (top 4 rows) and the real part (bottom 4 rows) of K_{ee}. Looking at entry 4(c) or 4(d) in Table IV, we find that $|\mathrm{Im}K_{ee}| < 0.13$, compared to the current best bound of 0.041, which is also the best bound for $|\mathrm{Im}K_{e\tau}|$, compared to our bound of 0.1 shown in Table V. Thus, an upgraded TEXONO experiment could provide independent confirmation of the bounds on these parameters, but would not probe new parameter space in the search for new physics. Similarly, as shown in Fig. 5 and Table V, the bounds on the FC semileptonic parameters $K_{e\mu}$ and $K_{e\tau}$ achievable by an upgraded TEXONO experiment are within a factor of 2 or 3 of the current bounds and possibly provide independent support, but not reach new regions in their parameter space.

Though the FC $K_{e\alpha}$ vs $\epsilon_{\alpha\mu}$ or $\epsilon_{\alpha\tau}$ studies, Fig. 5, provide no bounds on the ϵ_s because the "wrong flavor" source neutrinos are zero in the $K_{e\mu}$ or $K_{e\tau} \to 0$ limit, the $|\epsilon^{eR,L}_{\alpha e}|$ limits in Table IV apply to $|\epsilon^{eR,L}_{e\alpha}|$ because of the Hermiticity constraint $\epsilon^{eR,L}_{\alpha\beta} = (\epsilon^{eR,L}_{\beta\alpha})^*$, as noted after Eq. (3).

VI. SUMMARY AND CONCLUSIONS

We have explored the consequences of adding new physics effects at the reactor source in a $\bar{\nu} + e \to \bar{\nu} + e$ scattering experiment. We have used the data from the TEXONO experiment and also a model data based on their projected improved sensitivity in a future upgrade. This experiment has the virtue that its 30 m baseline does not allow for oscillation effects at the detector, so that any new physics at the source is not degenerate with oscillation effects during propagation. After developing the needed framework in Secs. II and III, where we explicitly include the NSI phases in the FC leptonic, detector parameters, we reviewed the 90% C.L. boundaries presented in Ref. [13] in Sec. IV, but included the phase effects on the boundary in the FC, $\epsilon^{eR}_{e\mu} - \epsilon^{eL}_{e\mu}$ parameter space. We checked that we properly reproduced the boundaries and the value, and statistical error of the TEXONO examples, but added the small but noticeable dependence on the choice of phases for the FC detector NSI parameters, filling a gap in the literature. The effects on the bounds one derives are at the 5% level. In lower energy experiments with sufficient statistics, this phase effect may be more striking as the coefficient of the correlation term becomes larger relative to the other terms contributing to the rate.

Including the NSIs at the reactor source, we surveyed examples of the interplay between the source and detector effects with a series of source vs detector 90% C.L. boundaries based on the TEXONO data. We find that the R-parameter bounds on the detector NSI parameters $\epsilon^{eR}_{\alpha e}$, $\alpha = e, \mu$, and τ, are about the same as the current best bounds, as summarized in Table VII from Ref. [11] in our Appendix B, but the corresponding L-parameter bounds are factors of 5 to 10 larger. All of the bounds on the source $K_{\alpha\beta}$ parameters are 1 to 2 orders of magnitude larger than best current bounds. Because the source FC parameters must be nonzero for a bound on the detector parameters $\epsilon^{eL,R}_{e\alpha}$ to exist, no meaningful bounds can be placed independently on the latter, but they differ only by a phase from the $\epsilon^{eL,R}_{\alpha e}$ parameters, as noted after Eq. (3), so the bounds on detector parameters listed in rows 2(c) and 2(d) in Table II apply as well to the detector parameters in rows 2(g) and 2(h) when α and $\beta = \mathrm{e}$.

Turning to the companion study of our model data based on the estimated future improvements in an upgraded TEXONO experiment, we basically repeated the exercises of Secs. III and IV to survey the parameter spaces in anticipation of this upgrade. Compared to the bounds based on current data our estimates of future, high sensitivity data show that an order of magnitude increase in the level of sensitivity to source and detector NSI parameters is achievable compared to the sensitivity with the current TEXONO data. This brings the bounds on detector NSI parameters well below current bounds in all but the case of $\epsilon^{eL}_{e\mu}$, which is the same as the current bound. Our new approach to bounding the CC, semileptonic NSIs at the source results in projected bounds that are comparable to the current ones. The very feature that makes this class of ultra-short-baseline experiments especially clean for probing the source NSI parameters, namely, the lack of interference with neutrino mixing amplitudes, makes it less sensitive. The parameters of interest appear as the modulus *squared* in the FC case, while in the NU case, the interference with the SM contribution gives a boost to the sensitivity to the real part of K_{ee}, which has a very tight bound already, coming from Cabibbo-Kobayashi-Maskawa (CKM) unitarity or lepton universality and for the same reason [11].

To conclude, we see that the currently envisaged upgrade to the TEXONO experiment promises to probe an order of magnitude deeper into the right-handed, leptonic NSI parameter space. To improve the sensitivity to the left-handed, leptonic NSI couplings, high intensity, short baseline ν_e experiments with large targets, along the lines of the LENA project [35,36] will be needed. To delve deeper into the semileptonic, CC parameter space with a reactor, antineutrino source, a third generation of the TEXONO-type of experiment would be needed, since we find that the current plans would only bring bounds to the level of those currently available. Otherwise, oscillation experiments with interference between the relevant NSI parameters and oscillation amplitudes involving standard oscillation parameters, independently measured and known to high accuracy would be needed, as remarked in Ref. [15].

ACKNOWLEDGMENTS

The authors are indebted to Dr. H. T. Wong and Dr. M. Deniz of the TEXONO Collaboration for their detailed communications. A. N. K. would like to thank The University of Kansas (KU) Particle Theory Group for hosting his visit while this work was begun, the HEC of Pakistan for supporting his graduate studies under the Indigenous PhD Fellowship Program (Batch-IV). D. W. M. and A. N. K received support from DOE Grant. No. De-FG02-04ER41308 and A. N. K also received partial support from the Saeeda-Iftikhar Scholarship award.

APPENDIX A: REACTOR NEUTRINO SPECTRUM AND EVENT RATE: THE TEXONO EXPERIMENT AT KUO-SHENG

The reactor antineutrinos spectrum produced at the Kuo-Sheng Nuclear Reactor is given in Fig. 6. We find the following fit function for the reactor neutrino spectrum between 3 and 8 Mev:

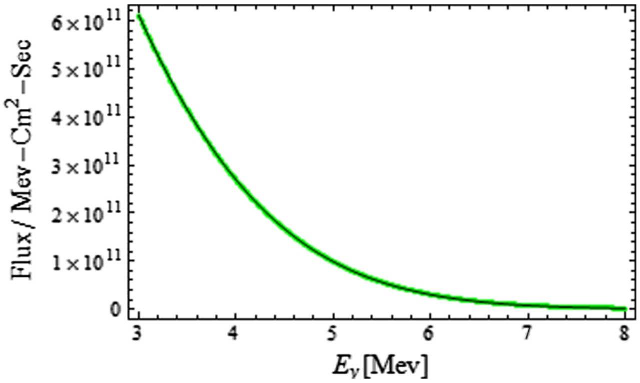

FIG. 6 (color online). Typical antineutrino spectrum at 28 m from the core at Kuo-Sheng. The green curve is the data and the black curve inside it is the fit.

$$\frac{d\phi(\bar{\nu}_e)}{dE_\nu} = \sum_0^6 \frac{a_n}{(E_\nu)^n} \tag{A1}$$

where the fit parameters $a_0, a_1 \ldots a_6$ have the values given in Table VI.

The experimentally observed event rate (R_E) is then compared with the theoretically modeled or expected event rate (R_X). The differential rate with respect to T, kinetic energy of the recoil electron, is

$$\frac{dR_X}{dT} = \rho_e \int_T^{E_\nu^{\max}} \mathcal{F}(E_\nu) \frac{d\phi(E_\nu)}{dE_\nu} dE_\nu, \tag{A2}$$

so the rate integrated over the ith bin in T is

$$R_X^i = \int_{T(i)}^{T(i+1)} \frac{dR_X}{dT}. \tag{A3}$$

Here ρ_e is the electron number density per kg of target mass of CsI(TI), and $\frac{d\phi(E_\nu)}{dE_\nu}$ is the neutrino spectrum as given in Eq. (A1) and $\mathcal{F}(E_\nu)$ is the factor containing the NSI detector cross sections and the corresponding NSI source parameter coefficients, as given in Eq. (7).

We use the following definition of χ^2 from Ref. [13] to perform the minimum-χ^2 fit,

$$\chi^2 = \sum_i \left(\frac{R_E^i - R_X^i}{\Delta_{\mathrm{stat}}^i} \right)^2, \tag{A4}$$

where R_E^i and R_X^i are the experimental and expected event rates over the ith data bin and Δ_{stat}^i is the corresponding statistical uncertainty of the measurement.

TABLE VI. Values of the fit parameters for the neutrino spectrum.

a_0	a_1	a_2	a_3	a_4	a_5	a_6
$-1.23779\ 10^{12}$	$3.72889\ 10^{13}$	$-4.38337\ 10^{14}$	$2.52571\ 10^{15}$	$-7.4559\ 10^{15}$	$1.11498\ 10^{16}$	$-6.74817\ 10^{15}$

APPENDIX B: BOUNDS OF REF. [11]

TABLE VII. Bounds at 90% C.L. taken from Eqs. (44) and (45) of Ref. [11] for comparison. Notice that we have used our notation for their bounds for convenience. It should be noted that there is a separate upper bound $\mathrm{Re}K_{ee} \sim 10^{-3}$ from the CKM unitarity and lepton universality constraints.

NSI parameters at source	NSI parameters at detector
$\lvert K_{ee}\rvert < 0.041$	$\lvert\varepsilon_{ee}^{eR}\rvert < 0.14$, $\lvert\varepsilon_{ee}^{eL}\rvert < 0.06$
...	$\lvert\varepsilon_{e\mu}^{eR}\rvert < 0.10$, $\lvert\varepsilon_{e\mu}^{eL}\rvert < 0.10$
...	$\lvert\varepsilon_{e\tau}^{eR}\rvert < 0.27$, $\lvert\varepsilon_{e\tau}^{eL}\rvert < 0.4$
$\lvert K_{e\mu}\rvert < 0.025$	$\lvert\varepsilon_{\mu e}^{eR}\rvert < 0.10$, $\lvert\varepsilon_{\mu e}^{eL}\rvert < 0.10$
...	$\lvert\varepsilon_{\mu\mu}^{eR}\rvert < 0.03$, $\lvert\varepsilon_{\mu\mu}^{eL}\rvert < 0.03$
...	$\lvert\varepsilon_{\mu\tau}^{eR}\rvert < 0.10$, $\lvert\varepsilon_{\mu\tau}^{eL}\rvert < 0.10$
$\lvert K_{e\tau}\rvert < 0.041$	$\lvert\varepsilon_{\tau e}^{eR}\rvert < 0.27$, $\lvert\varepsilon_{\tau e}^{eL}\rvert < 0.4$
...	$\lvert\varepsilon_{\tau\mu}^{eR}\rvert < 0.10$, $\lvert\varepsilon_{\tau\mu}^{eL}\rvert < 0.10$
...	$\lvert\varepsilon_{\tau\tau}^{eR}\rvert < 0.4$, $\lvert\varepsilon_{\tau\tau}^{eL}\rvert < 0.16$

[1] Y. Abe *et al.* (Double Cooz Collaboration), Phys. Rev. Lett. **108**, 131801 (2012); Phys. Rev. D **86**, 052008 (2012).

[2] F. An *et al.* (Daya Bay Collaboration), Phys. Rev. Lett. **108**, 171803 (2012); Chin. Phys. C **37**, 011001 (2013).

[3] J. Ahn *et al.* (RENO Collaboration), Phys. Rev. Lett. **108**, 191802 (2012).

[4] K. Abe *et al.* (Super Kamiokande Collaboration), Phys. Rev. Lett. **112**, 091805 (2014).

[5] P. Adamson *et al.* (MINOS Collaboration), Phys. Rev. Lett. **112**, 191801(2014).

[6] For example, the MINOS experiment has constrained the $\mu - \tau$ FC, NC parameter [7], which affects the propagation of ν_μ, while Ref. [8] finds an allowed range of NSI parameters that allow the differing central values for $\sin^2(2\theta_{13})$ measured by [4] and [2] to be compatible with each other, even if their central values remain unchanged as their uncertainties shrink.

[7] P. Adamson *et al.* (MINOS Collaboration), Phys. Rev. D **88**, 072011 (2013).

[8] I. Girardi, D. Meloni, and S. Petcov, Nucl. Phys. **B886**, 31 (2014).

[9] Y. Grossman, Phys. Lett. B **359**, 141 (1995). This paper is the first to introduces the idea and achieves the first bounds.

[10] T. Ohlsson, Rep. Prog. Phys. **76**, 044201 (2013). The author reviews the status of NSIs through 2012.

[11] C. Biggio, M. Blennow, and E. Fernandez–Martinez, J. High Energy Phys. 08 (2009) 090.

[12] M. Deniz *et al.* (TEXONO Collaboration), Phys. Rev. D **81**, 072001 (2010).

[13] M. Deniz *et al.* (TEXONO Collaboration), Phys. Rev. D **82**, 033004 (2010).

[14] Y.-F. Li, Int. J. Mod. Phys. Conf. Ser. **31**, 1460300 (2014).

[15] A. N. Khan, D. W. McKay, and F. Tahir, Phys. Rev. D **88**, 113006 (2013).

[16] T. Ohlsson, H. Zhang, and S. Zhou, Phys. Lett. B **728**, 148 (2014).

[17] I. Girardi and D. Meloni, arXiv:1403.5507.

[18] S. Davidson, C. Pena-Garay, N. Rius, and A. Santamaria, J. High Energy Phys. 03 (2003) 011.

[19] J. Barranco, O. G. Miranda, C. A. Moura, and J. W. F. Valle, Phys. Rev. D **77**, 093014 (2008).

[20] J. Barranco, O. G. Miranda, C. A. Moura, and J. W. F. Valle, Phys. Rev. D **73**, 113001 (2006).

[21] D. V. Forero and M. M. Guzzo, Phys. Rev. D **84**, 013002 (2011).

[22] J. Kopp, M. Lindner, T. Ota, and J. Sato, Phys. Rev. D **77**, 013007 (2008).

[23] T. Ohlsson, Rep. Prog. Phys. **76**, 044201 (2013).

[24] J. M. Conrad, M. H. Shaevitz, I. Shimizu, J. Spitz, M. Toups, and L. Winslow, Phys. Rev. D **89**, 072010 (2014). This paper outlines the IsoDAR source's potential for improved measurements of $\sin^2\theta_W$ and limits on ϵ_{ee}^{eL} and ϵ_{ee}^{eR} from $\bar{\nu}_e - e$ elastic scattering.

[25] M. Deniz, S. Bilmis, and H. T. Wong, J. Phys. Conf. Ser. **375**, 042044 (2012).

[26] L. M. Johnson and D. W. McKay, Phys. Lett. B **433**, 355 (1998).

[27] L. M. Johnson and D. W. McKay, Phys. Rev. D **61**, 113007 (2000).

[28] D. McKay and L. Johnson, in *Proceedings of PASCOS99, Lake Tahoe*, edited by K. Cheung, J. Gunion, and S. Mrenna (World Scientific, Singapore, 2000), pp 204–207.

[29] S. Bergmann and Y. Grossman, Phys. Rev. D **59**, 093005 (1999).

[30] M. C. Gonzalez-Garcia, Y. Grossman, A. Gusso, and Y. Nir, Phys. Rev. D **64**, 096006 (2001).

[31] We thank Dr. H. T. Wong and Dr. M. Deniz of the TEXONO Collaboration for sharing these data with us.

[32] G. Bellini *et al.* (Borexino Collaboration), Phys. Rev. D **89**, 112007 (2014).

[33] For cases where there is no systematic correlation between parameters, the one-parameter and two-parameter bounds on the individual parameters are the same anyway.

[34] J. Erler and M. J. Ramsey-Musolf, Phys. Rev. D **72**, 073003 (2005).

[35] M. Wurm *et al.* (LENA Collaboration), Astropart. Phys. **35**, 685 (2012).

[36] E. A. Garcés, O. G. Miranda, M. A. Tórtola, and J. W. F. Valle, Phys. Rev. D **85**, 073006 (2012).